UNIVERSITÁ DEGLI STUDI DI PADOVA

Dipartimento di Fisica e Astronomia "Galileo Galilei"

Final Report

Bachelor's Degree in Physics

PULSE SHAPE DISCRIMINATION OF THE GERMANIUM DETECTORS OF THE LEGEND-200 EXPERIMENT

PULSE SHAPE DISCRIMINATION DEI RIVELATORI AL GERMANIO DELL'ESPERIMENTO LEGEND-200

SUPERVISOR:
Prof. Riccardo Brugnera

CO-SUPERVISORS:
Dott.ssa Sofia Calgaro
Dott.ssa Giovanna Saleh

CANDIDATE:
Stefano Abaribbi
mat. 2008003

Academic Year: 2023-2024

Abstract - IT

Il decadimento doppio beta senza neutrini ($0\nu\beta\beta$) è un processo ipotetico che viola la conservazione del numero leptonico. Le implicazioni della sua osservazione sono molteplici e di vasta portata: dalla violazione della conservazione del numero leptonico totale, alla definzione della natura del neutrino (di Majorana o di Dirac), al fornire un vincolo alla massa assoluta dei neutrini, all'aiutare a capire l'asimmetria tra materia e antimateria presente nel nostro universo. LEGEND e' un esperimento dedicato alla ricerca del decadimento doppio beta senza neutrini utilizzando come nucleo attivo il ^{76}Ge. La prima fase, quella in corso, prende il nome di LEGEND-200 in quanto opera con 200kg di germanio ed è a partire dai dati raccolti in questo primo anno di attività che è stata scritta questa tesi.

L'obiettivo è quello di provare l'efficienza della Pulse Shape Discrimination: tecnica utilizzata per ridurre gli eventi di background nell'esperimento. In particolare si è dapprima analizzata su dati di calibrazione la risposta dei detector alla PSD e la sua stabilità nel tempo. Successivamente si è fatto un confronto fra la sua applicazione in LEGEND-200 e in GERDA, precursore di LEGEND, che ha terminato l'attività alla fine del 2019.

Abstract - EN

Neutrinoless double-beta decay ($0\nu\beta\beta$) is a hypothetical process that violates lepton number conservation. The implications of its observation are multiple and far-reaching: from violating the conservation of the total lepton number, to defining the nature of the neutrino (Majorana or Dirac), to providing a constraint on the absolute mass of neutrinos, to helping to understand the asymmetry between matter and antimatter present in our universe. LEGEND is an experiment dedicated to the search for neutrinoless double-beta decay using ^{76}Ge as active nucleus. The current phase, known as LEGEND-200, operates with 200 kg of germanium and this thesis is based on the data collected during its first year of operation.

The purpose of this thesis is to test the efficiency of Pulse Shape Discrimination (PSD), a technique used to minimize background events in the experiment. Initially, the response of the detectors to PSD was tested using calibration data and its stability over time was evaluated. Subsequently, a comparison was made between its application in LEGEND-200 and in GERDA, the predecessor of LEGEND, which concluded its activities at the end of 2019.

Contents

1 Neutrinoless double-beta decay theory

Double-beta decay is a rare decay process that involves the transformation of two neutrons in the atomic nucleus into protons (or vice versa), with the emission of two β particles (electrons or positrons depending on the type of decay, just like in single beta decay). In the following discussion, we will refer exclusively to β^- decays which, in the case of single decay, are characterized by the transformation of a neutron into a proton with the emission of an electron and an electron antineutrino ($n \rightarrow p + e^- + \bar{\nu}_e$). The complementary decay can be treated similarly.

First of all, two types of double-beta decay have been theorized:

- Two-neutrino double-beta decay ($2\nu\beta\beta$): $(A, Z) \rightarrow (A, Z+2) + 2e^- + 2\bar{\nu}_e + Q_{\beta\beta}$
- Neutrinoless double-beta decay ($0\nu\beta\beta$): $(A, Z) \rightarrow (A, Z+2) + 2e^- + Q_{\beta\beta}$

The first one is a decay predicted by the Standard Model, whose existence has been confirmed by laboratory observations in the late 1980s. The measured half-life spans the energy range from $10^{18}y$ to $10^{22}y$. As shown by the mass parabolas in *Figure 1.1*, this decay characterizes particularly stable even-even nuclei which, however, present even more stable even-even isobars. Since beta decay to the next odd-odd nucleus is prohibited due to the higher mass, the nucleus is forced to decay directly to the even-even one; this decay is balanced by the emission of two beta particles and their corresponding electron antineutrinos.

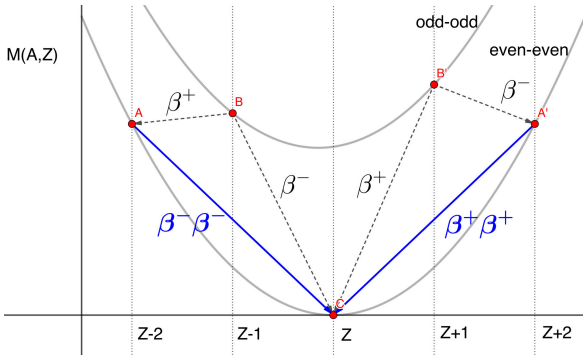

Figure 1.1: *Mass parabolas for double-beta decay*

The neutrinoless double-beta decay, on the other hand, exhibits a clear violation of the Standard Model, namely the non-conservation of the total lepton number. It is evident that, without the two neutrinos with a total lepton flavor of -2, the total lepton number of the electrons (+2) is not balanced. Consequently, this is a decay where $\Delta L = 2$.

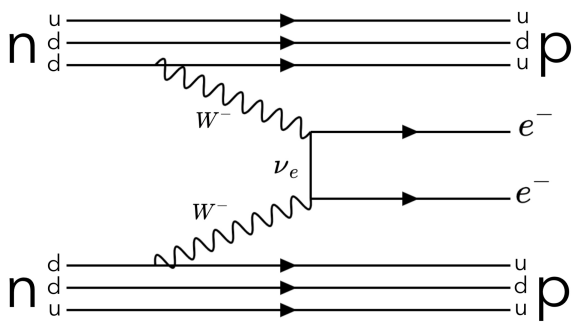

Figure 1.2: *Feynmann diagram of* $0\nu\beta\beta$ *decay*

This violation of the Standard Model can be understood assuming the neutrino as massive Majorana particles. In the Majorana theory, neutrino coincides with its antineutrino partner. The *Figure 1.2* shows how the neutrinoless double-beta decay can be understood following this hypothesis.

The experimental observation of neutrino flavor oscillations made by Super-Kamiokande in 1998 opened up the possibility that Majorana's theory might be correct [1]. In fact the oscillations of the neutrinos can be understood assuming that the neutrinos have mass, in contrast with the assumption of zero mass in the Standard Model, and leaving the possibility of a violation of the lepton flavor numbers. The search for neutrinoless double-beta decay and the consequent violation of total lepton number thus constitute a fundamental piece in understanding physics beyond the Standard Model. To date, there are no experimental observations of this phenomenon, whose half-life has been estimated to be $> 10^{26}$ years.

2 Experimental setup

The Large Enriched Germanium Experiment for Neutrinoless Double Beta Decay (LEGEND) is an experimental project located at the Gran Sasso National Laboratories (LNGS) of INFN dedicated to the search for the $0\nu\beta\beta$ decay of the ^{76}Ge. The development of this project consists of two phases, LEGEND-200 and LEGEND-1000. During these phases, germanium detectors with a total mass of $200kg$ and $1000kg$ respectively will be used. This work will provide only information related to LEGEND-200 as it is the phase currently underway.

The goal pursued in designing the setup of this experiment, given the rarity of the searched decay, is to highly suppress background events coming from the surrounding environment. To achieve this purpose, LEGEND relies on the well-established technologies of GERDA (GERmanium Detector Array) and the MAJORANA DEMONSTRATOR experiment. The experimental structure used by LEGEND-200 is the pre-existing one from GERDA and is visible in *Figure 2.1*. The setup consists of 12 strings of germanium diodes, a cryostat with liquid argon (LAr), a tank of ultra-pure water on which 66 photomultipliers (PMT) are placed, and a clean room above the cryostat and the water tank.

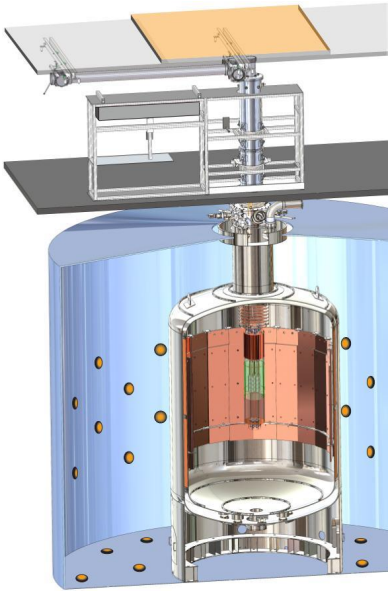

Figure 2.1: *Experimental setup. Picture from [2]*

DETECTORS - LEGEND-200 uses 4 types of detectors: *p-type point-contact detectors* (PPC), *broad-energy Ge detectors* (BEGe), *p-type inverted-coaxial point-contact detectors* (ICPC) and *semicoaxial detectors* (COAX). These detectors differ in shape and mass. They are all made of high-purity germanium enriched from 86% to 92% of ^{76}Ge (in natural germanium, the percentage of ^{76}Ge is approximately 7.8%). Depending on the shape and size, the two electrodes assume different structures. For the first three types of germanium detectors the shapes are shown in *Figure 2.2*, here the p^+ electrode is much smaller than the n^+ electrode, ensuring a high gradient for the electric potential near the p+ electrode. The fact that source and detectors are equal is also a reason for high detection efficiency. Another noteworthy element is the presence of 4

radioactive sources made of ^{228}Th that can be inserted among the detectors for calibration purposes. A view of the internal part of the detector can be seen in *Figure 2.3*.

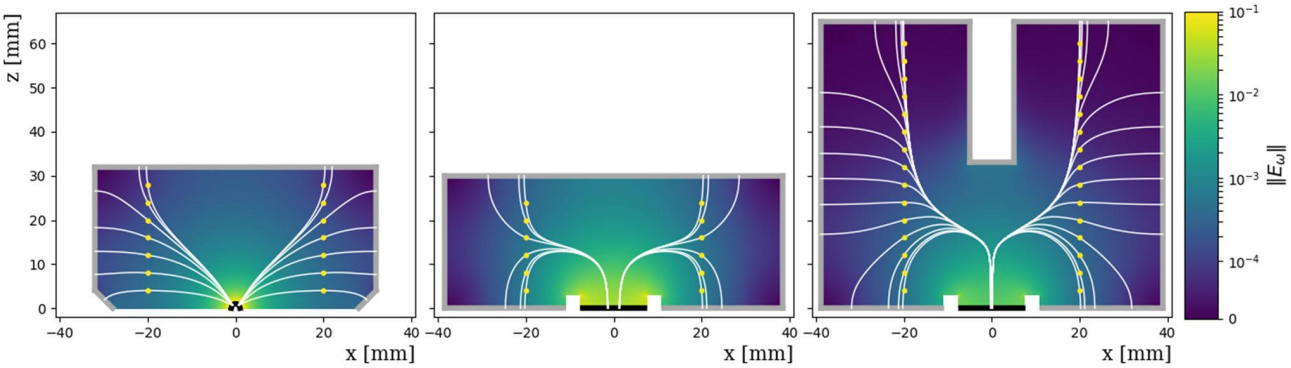

Figure 2.2: *Electric field lines in the section of the three detector types (from left to right: PPC, BEGe, ICPC). The thick black line represents the p^+ electrode, while the gray line represents the n^+ electrode. Picture from [3]*

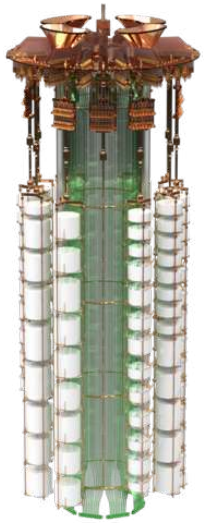

Figure 2.3: *View of the internal part of the detector*

CRYOSTAT - The germanium detectors operate immersed in 64m^3 of liquid argon (LAr). This serves three purposes: firstly, the cryogenic temperatures prevent valence band electrons from being promoted to the conduction band and interfering with the signal; secondly, as a further shield against the remnants of the external gamma background penetrating the surrounding water and against the radioactivity of the cryostat itself; thirdly, argon has scintillation properties that allow to use it as active veto tool. Through fibers positioned in two concentric circles around the detectors (see *Figure 2.3*), it is possible to capture the scintillation light produced by ionizing radiation interacting with LAr. The cryostat structure is made of stainless steel, internally coated with copper. The copper serves as a shield for γ radiation coming from the steel.

WATER TANK - The cryostat is also immersed in a 590m^3 ultra-pure water tank, which serves as additional shield. In particular, the use of water as veto is related to the Cherenkov light emitted by energetic particles (especially muons, given the depth at which the experiment is located) passing through the tank. This light is detected by the 66 PMTs placed on the walls.

CLEAN ROOM - Above the neck of the cryostat, there is a clean room containing the system (called lock) that allows lowering the detectors inside the cryostat.

3

PSD analysis on calibration data

3.1 The Pulse Shape Discrimination

As previously noted, no neutrinos are released during a $0\nu\beta\beta$ decay. This characteristic is fundamental in the search for this decay because it ensures that the energy spectrum obtained by summing the energies of the two electrons is not continuous (as it is in $2\nu\beta\beta$, where the energy is randomly distributed among electrons and neutrinos) but rather characterized by a monoenergetic peak at the value of $Q_{\beta\beta}$. For this reason, experiments like LEGEND-200 aim to achieve a signal cleanliness that allows for the observation of this peak.

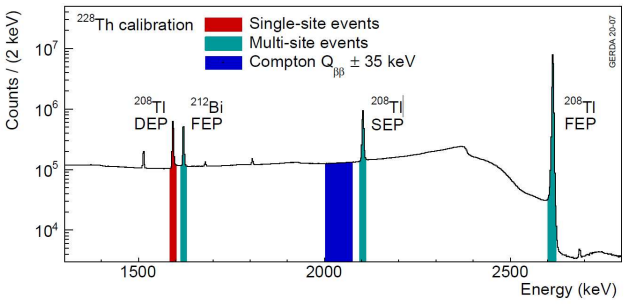

Figure 3.1: *Calibration spectrum. Picture from [4]*

Pulse Shape Discrimination (PSD) is one of the techniques used to remove background events from the signal. This technique is trained using calibration data that are acquired thanks to ^{228}Th sources. The energy spectrum of the calibration data is shown in *Figure 3.1*, where the regions of interest for PSD analysis are also highlighted. In particular, we observe: at 1593 keV the Double Escape Peak (DEP) of ^{208}Tl; at 1621 keV the Full Energy Peak (FEP) of ^{212}Bi; at 2104 keV the Single Escape Peak (SEP) of ^{208}Tl; and at 2615 keV the Full Energy Peak (FEP) of ^{208}Tl. Additionally, in the $Q_{\beta\beta} \pm 35$ keV range, a Compton Continuum region is used to estimate the background rejection in the region of interest. The importance of these peaks is related to their nature: while the ^{208}Tl DEP is characterized by Single-Site Events (SSE), analogous to the sought-after $0\nu\beta\beta$ decay, the other peaks are characterized by Multi-Site Events (MSE). Applying PSD to calibration data thus allows us to estimate its ability to distinguish between these two types of events.

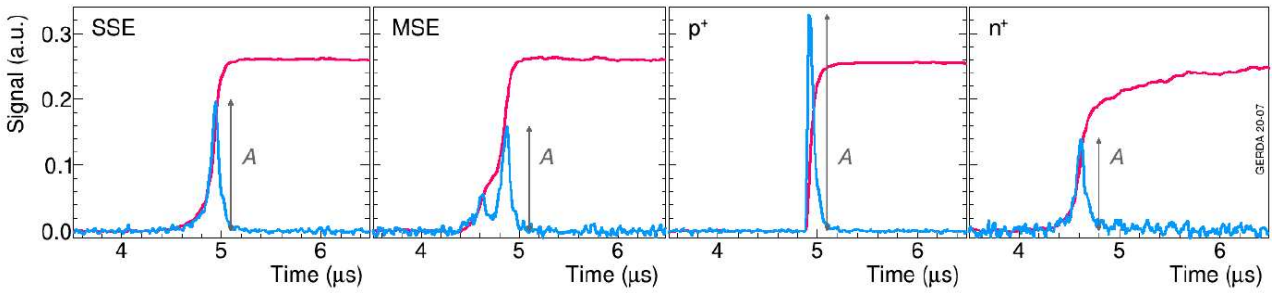

Figure 3.2: *Charge pulses (red) and derived current pulses (blue) from a BEGe detector. From left to right: an SSE, an MSE, an event near the p^+ electrode, and an event near the n^+ electrode with partial charge collection. Picture from [4]*

To achieve this, a parameter is calculated from the shape of the charge pulse coming from the detectors. As shown in *Figure 3.2*, different types of signals are characterized by different pulse shapes. These differences are quantified using the A/E (or AoE) parameter, calculated from the amplitude A of the pulse and the energy E associated with it (the details of this calculation are not relevant to this report). A lower A/E cut serves to remove MSEs and n^+ surface events and it is set to achieve a 90% Survival Fraction for the DEP. An upper cut is intended to discard p^+ surface events. This makes the PSD filter a "double-sided cut." It is also noted that this type of PSD analysis, based on the A/E cut method, is valid only for three types of detectors: BEGe, ICPC, and PPC. Consequently, the following discussion will focus on these types of detectors and exclude COAX from the analysis.

3.2 Calculation of the Survival Fractions

In this section, we demonstrate the technique used to calculate the Survival Fractions (SF) in the regions of the ^{208}Tl DEP, the ^{212}Bi FEP, and the Compton Continuum (CC) after the application of PSD filters. As an example to demonstrate the effects of PSD on the three regions of the spectrum, data from an ICPC-type detector (specifically ch1104000) were used. In *Figure 3.3*, the energy spectrum between 0 keV and 3000 keV is shown after applying a preliminary cut to eliminate any "non-physical" events. The two peaks on which PSD will be tested are also highlighted.

Firstly, it is necessary to subtract the background from the signal. This is achieved by considering the left and right side bands of the peak of interest, where no other peaks are present. The average background is calculated from these side bands and, assuming that the background does not vary significantly within the peak region, the mean of the two side band values is subtracted from the counts within the peak region. Subsequently, the PSD double-sided-cut is applied to the data. The Survival Fraction is then calculated as $SF = \frac{N_{psd}}{N_{tot}}$, where N_{psd} is the number of events surviving the PSD cut, and N_{tot} is the total number of events. The differences between the results obtained for the ^{208}Tl DEP and ^{212}Bi FEP are shown in *Figure 3.4.*

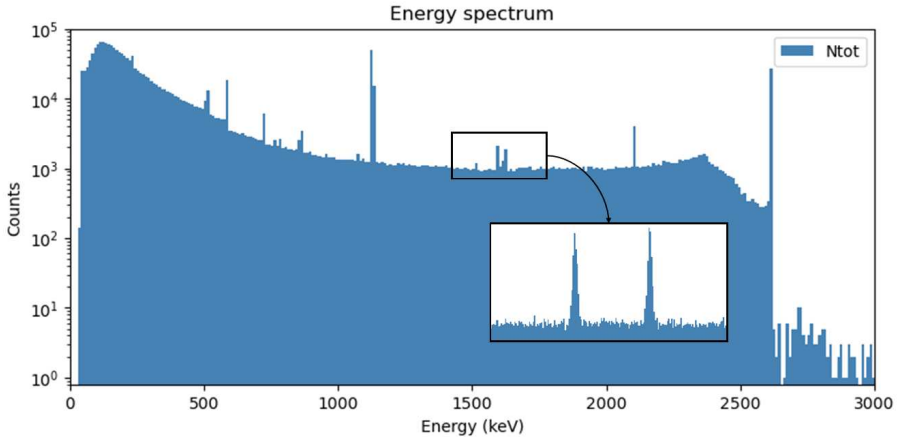

Figure 3.3: *Energy spectrum of ch1104000 in period p09 and focus on the region with ^{208}Tl DEP and ^{212}Bi FEP*

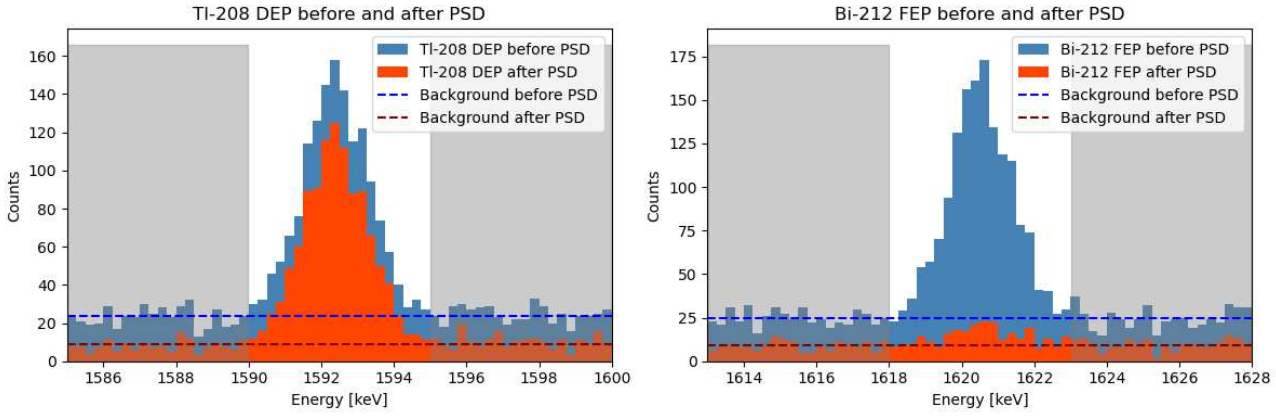

Figure 3.4: *Comparison of the application of the PSD cut on the ^{208}Tl DEP and on the ^{212}Bi FEP*

For the ^{208}Tl DEP, the Survival Fraction is $SF_{DEP} = 0.86 \pm 0.01$. This result aligns with expectations as the AoE-low-side-cut is set to retain 90% of events, while the AoE-high-side-cut contributes by slightly reducing the SF value. Regarding the ^{212}Bi FEP, the Survival Fraction obtained is $SF_{FEP} = 0.088 \pm 0.008$, indicating that most of the peak events have been removed, consistent with expectations (i.e. a peak made mainly of multi-site events).

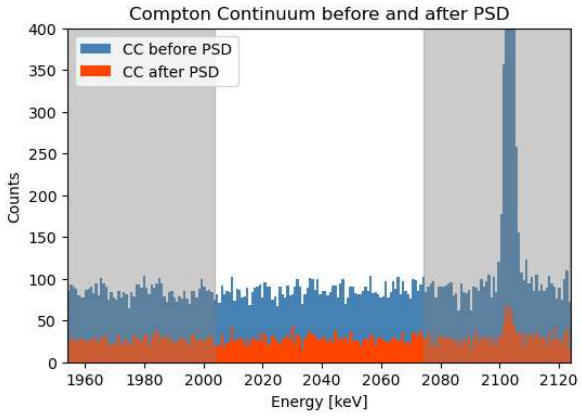

Figure 3.5: *Application of PSD in the CC region*

In addition to the two peaks, the Survival Fraction is also calculated in the Compton Continuum region $Q_{\beta\beta} \pm 35$ keV. This is done to evaluate the performance of PSD in the region of interest and, extending this analysis to all detectors and over longer time periods, allows for assessing its efficiency and stability over time. In *Figure 3.5*, the comparison between the spectrum before and after applying the PSD filter can be observed, resulting in a Survival Fraction of $SF_{CC} = 0.322 \pm 0.006$.

3.3 Survival Fractions VS Detector Mass

A preliminary investigation to test the rejection capabilities of the detectors was conducted by applying the procedure described in the previous section to the spectrum collected from each detector. The sets of three Survival Fractions were then sorted according to the detector mass, as presented in *Figure 3.6* for ICPC detectors, *Figure 3.7* for BEGe detectors, and *Figure 3.8* for PPC detectors:

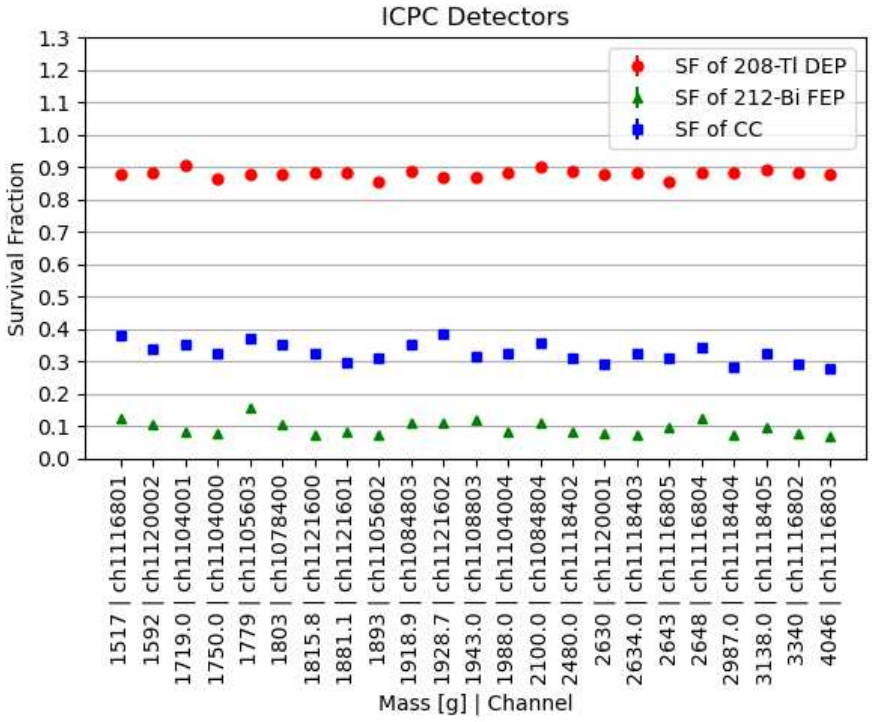

Figure 3.6: *Survival Fractions of the ^{208}Tl DEP, ^{212}Bi FEP, and CC($Q_{\beta\beta}$) for the active ICPC detectors in p09, sorted by mass. The uncertainties are smaller than the markers*

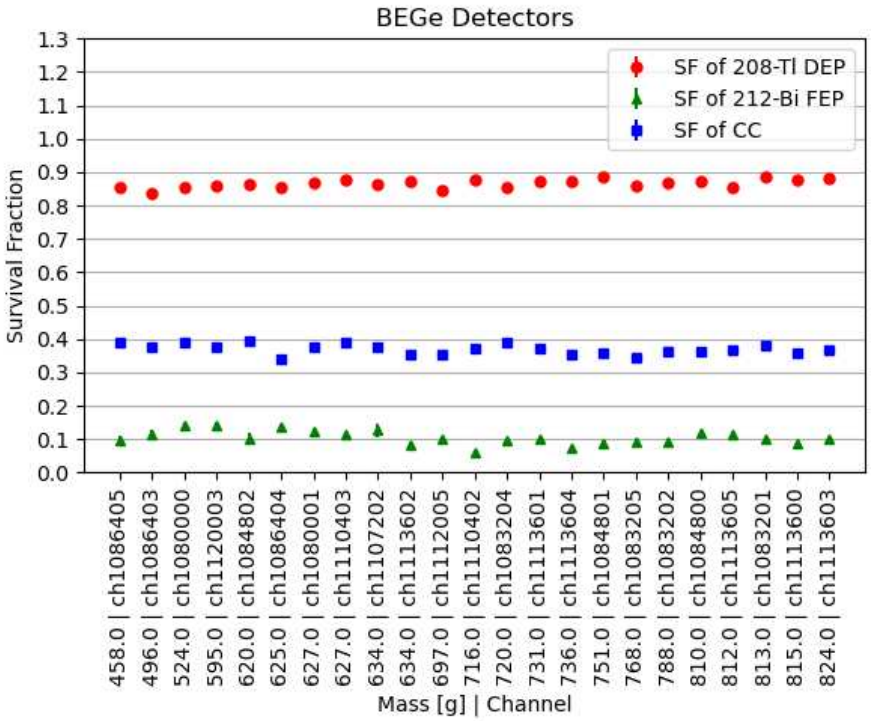

Figure 3.7: *Survival Fractions of the ^{208}Tl DEP, ^{212}Bi FEP, and CC($Q_{\beta\beta}$) for the active BEGe detectors in p09, sorted by mass. The uncertainties are smaller than the markers*

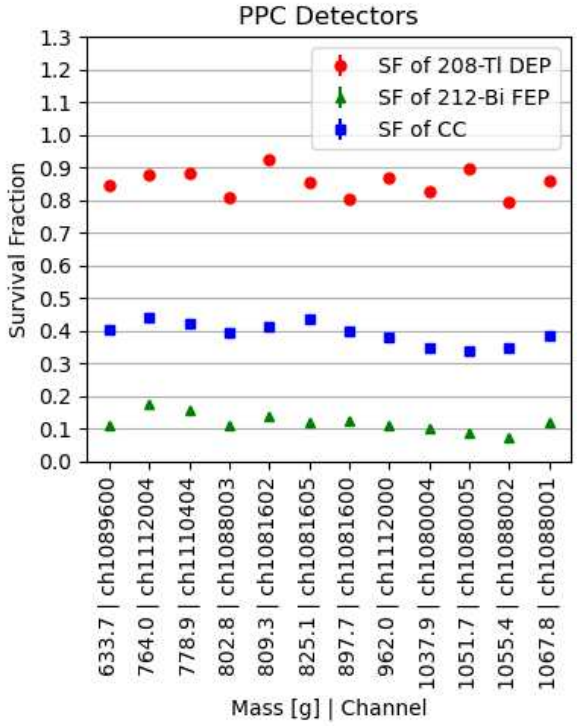

Figure 3.8: *Survival Fractions of the ^{208}Tl DEP, ^{212}Bi FEP, and CC($Q_{\beta\beta}$) for the active PPC detectors in p09, sorted by mass. The uncertainties are smaller than the markers*

Firstly, it is important to specify that, as mentioned earlier, COAX-type detectors were not considered. Similarly, some detectors of the three analyzed types were excluded because they did not meet certain operational requirements which were detected run-by-run by the system and reported in the LEGEND-200 Metadata.

From these graphs, a substantial consistency can be observed in the results obtained from the three types of detectors regarding their ability to discriminate SSEs from MSEs. Moreover, the choice to order them by mass is not by chance. Indeed, higher masses correspond to larger volumes and, consequently, higher probabilities of registering MSEs. For this reason, a progressive decrease in the Survival Fraction with increasing mass is expected. This variation is not noticeable in BEGe and PPC detectors, likely due to the limited range of mass values for these types of detectors. In contrast, a slight decrease in the Survival Fraction is observed among ICPC detectors: for lighter ones, it fluctuates around 35%, while for heavier ones, it hovers around 30%. Unfortunately, the oscillations in SF values for the various detectors are too high to analyze this phenomenon in more detail. For such analyses, it would be more appropriate to average SF values over longer time periods, such as over all periods of the prod-cycle rather than just one. However, for now, only p09 data has been used because hardware changes between periods are quite significant, and it would not be advisable to combine data from multiple periods into a single statistical sample. Nevertheless, further considerations on the mass-SF correlation are discussed in Section 3.5.

3.4 Survival Fractions VS detector positions

A second assessment of the quality of PSD in LEGEND-200 stems from an issue previously identified in GERDA. It was observed that there existed a correlation between Survival Fraction and the position of detectors within the strings. As depicted in *Figure 3.9* (taken from the article "*Pulse shape analysis in GERDA Phase II*" [4]), an increase in the distance between the front-end electronics and the detectors (i.e. longer cables) led to an increase in the Survival Fraction of the ^{212}Bi FEP and the $Q_{\beta\beta}$ Compton Continuum. This issue was attributed to the layout of GERDA's electronics, which were subsequently modified for LEGEND-200. To verify if this problem had been resolved, the set of two of Survival

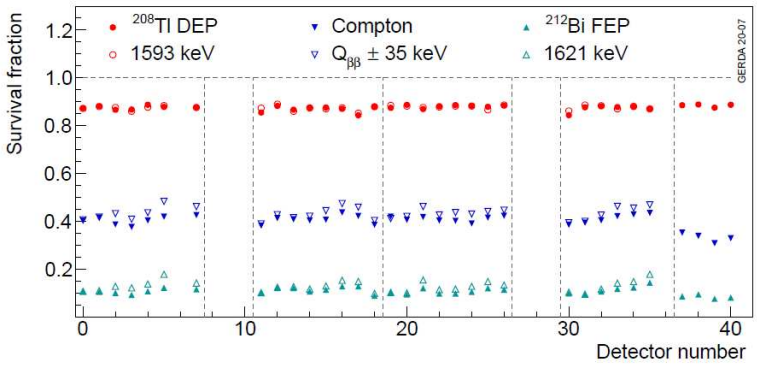

Figure 3.9: *Survival Fractions of the ^{208}Tl DEP, ^{212}Bi FEP, and CC($Q_{\beta\beta}$) in GERDA. The black lines separate the strings; the error bars are smaller than the markers. Image from [4]*

Fractions for all active detectors during the p09 period were sorted by their positions in the strings. The result is shown in *Figure 3.10*. Note that some strings have fewer detectors due to exclusions explained in the previous paragraph (in particular, string 2 predominantly consists of COAX-type detectors, which were excluded from the analysis).

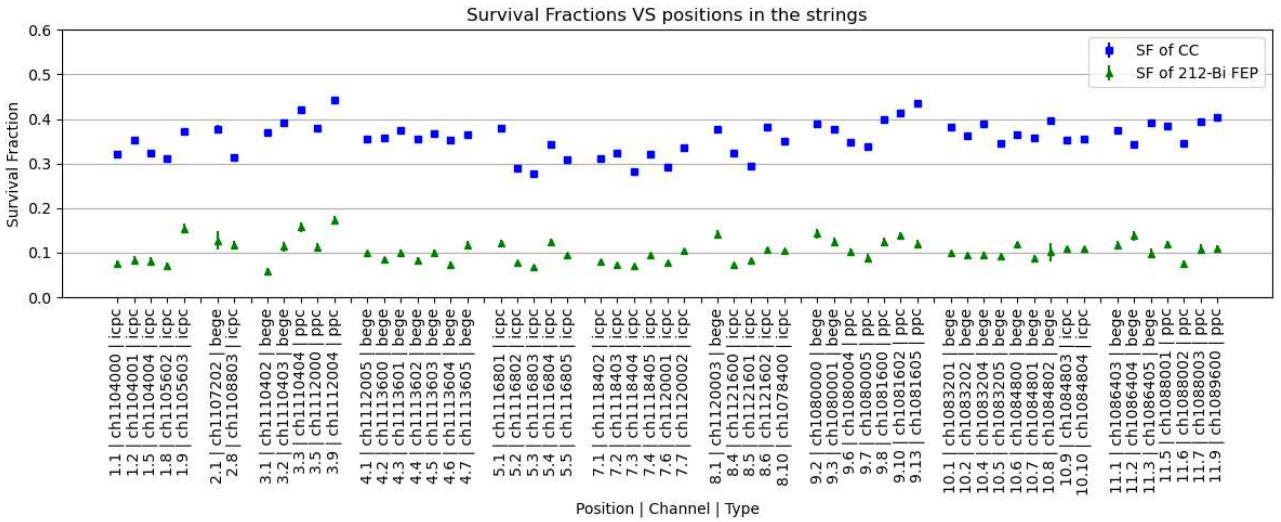

Figure 3.10: *Survival Fractions of the ^{208}Tl DEP, ^{212}Bi FEP, and CC($Q_{\beta\beta}$) for all active detectors in p09, sorted by their position in the strings. The error bars are smaller than the markers.*

From the graph, it can be seen that the correlation observed in GERDA is no longer present in LEGEND-200. The only string where there is a noticeable increasing trend in Survival Fractions is string number 3. However, it is difficult to ascertain whether this trend is random or attributable to some instrumental issue, given that only 5 out of 9 detectors in the string pass checks for proper functioning. The absence of this trend in the other strings suggests that this correlation has been solved in LEGEND-200.

3.5 Stability of PSD over Time

An additional test to verify the functionality of PSD concerns its stability over time. To assess this, a different approach was taken compared to the method described earlier. Instead of calculating the Survival Fractions detector by detector using data acquired over an entire period, the analysis was conducted run by run by combining the data from all detectors of a certain type into a single dataset. This was done to examine the stability of SF values over a nearly one-year time span. The results obtained for the three types of detectors are shown in *Figure 3.11*, *Figure 3.12*, and *Figure 3.13* for ICPC, BEGe, and PPC respectively. The start dates and end dates of each period are detailed in *Table 3.1*.

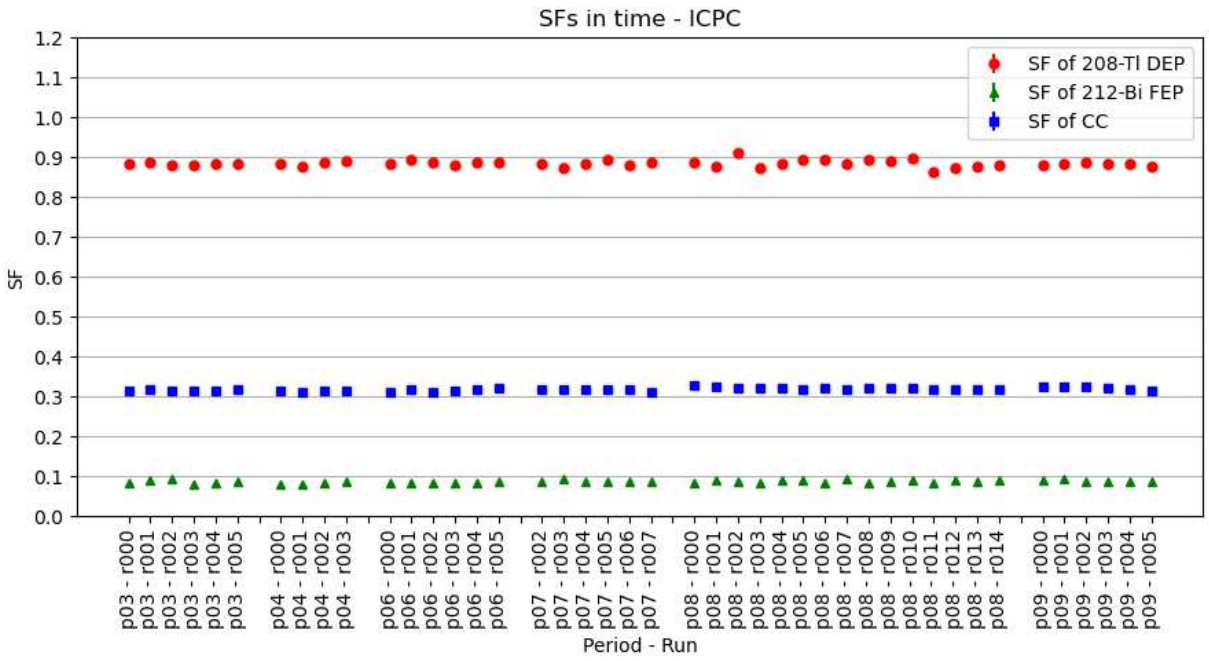

Figure 3.11: *Survival Fractions of the ^{208}Tl DEP, ^{212}Bi FEP, and CC($Q_{\beta\beta}$) calculated for all active ICPC detectors run by run. The error bars are smaller than the markers.*

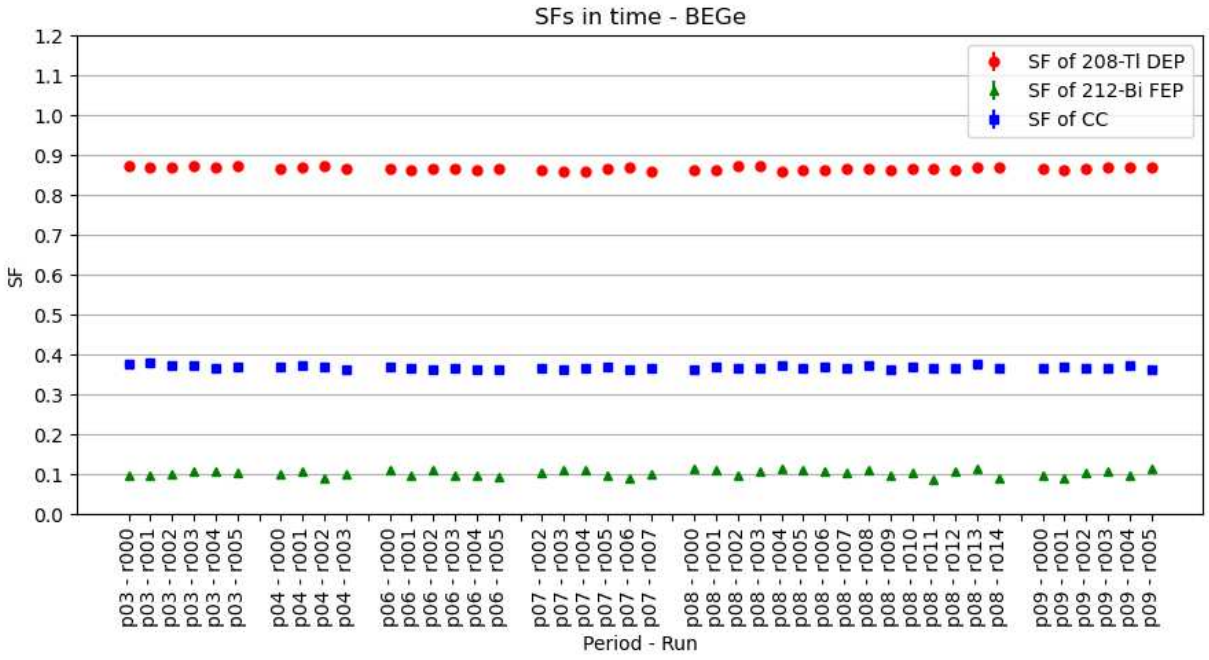

Figure 3.12: *Survival Fractions of the ^{208}Tl DEP, ^{212}Bi FEP, and CC($Q_{\beta\beta}$) calculated for all active BEGe detectors run by run. The error bars are smaller than the markers.*

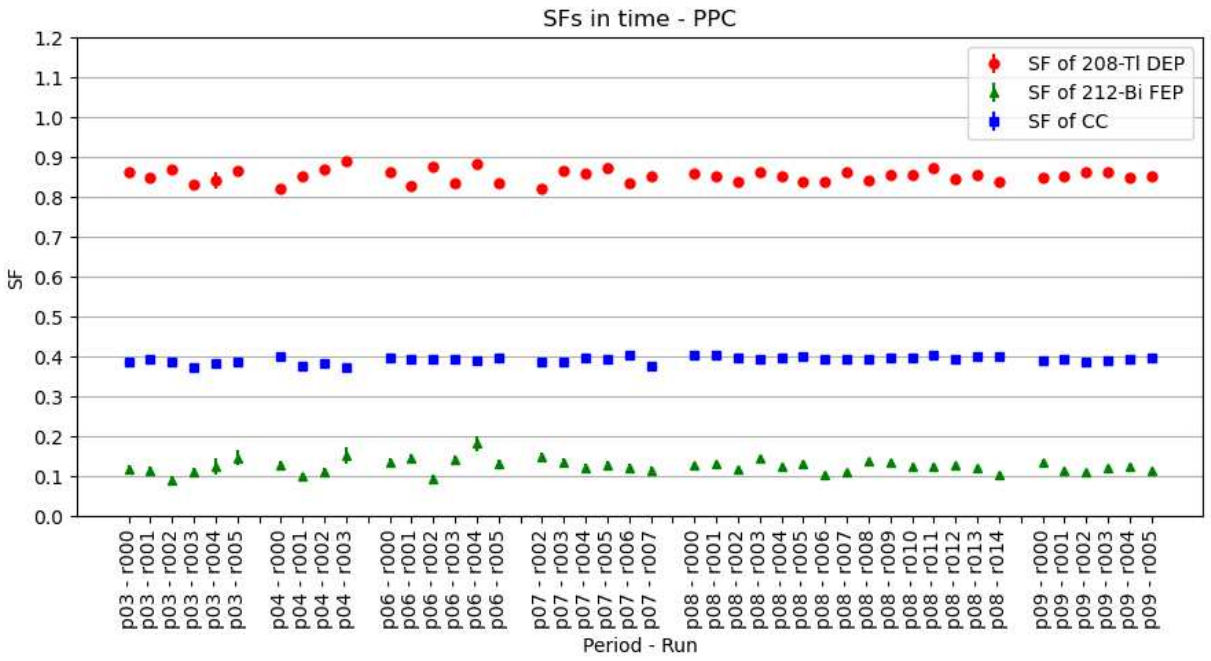

Figure 3.13: *Survival Fractions of the ^{208}Tl DEP, ^{212}Bi FEP, and CC($Q_{\beta\beta}$) calculated for all active PPC detectors run by run. The error bars are smaller than the markers.*

Period	Start date	End date
p03	2023/03/11	2023/04/12
p04	2023/04/14	2023/05/01
p06	2023/06/11	2023/07/17

Period	Start date	End date
p07	2023/08/14	2023/09/18
p08	2023/10/02	2024/01/01
p09	2024/01/10	2024/02/12

Table 3.1: *Start and end dates of the data acquisition periods*

From this analysis, the expected time stability emerges clearly, notably with minimal oscillations, especially in the BEGe and ICPC detectors. Another interesting point, as mentioned in paragraph 3.3, is that the Survival Fractions of the CC($Q_{\beta\beta}$) assume markedly different values for ICPC ($\sim$32%), BEGe ($\sim$37%), and PPC ($\sim$39%). This result is anticipated and is due to the significantly larger volume of ICPC detectors, as seen in *Figure 2.2*. Therefore, although it may be challenging to observe a progressive decrease in Survival Fractions with increasing mass of detector of the same type, this correlation becomes evident when averaging across all detectors and comparing the differences in Survival Fractions between different types of detectors.

4 Comparison of PSD in GERDA and in LEGEND-200

To conclude this discussion, the effect of applying PSD on LEGEND-200 physics data was compared with that on GERDA data. This was done by keeping separated the data for the different types of detectors, specifically using only BEGe and ICPC since there were no PPC detectors in GERDA. The energy spectra of GERDA are presented in *Figure 4.1* and *Figure 4.2*, while those of LEGEND are shown in *Figure 4.3* and *Figure 4.4*. Note that no cuts related to the Liquid Argon Veto were applied to any of these spectra as the study of this filter is not of interest in this discussion. Therefore, the reference energy spectra only consider PSD cuts.

For each of these spectra, presented as histograms with a bin width of 15keV, the bin-by-bin ratio between the counts after and the counts before the application of PSD was also calculated. By observing the trend of these ratios, it is possible to compare the rejection capability of PSD in various regions of the spectrum. The results of these ratios are presented in *Figure 4.5* for GERDA and in *Figure 4.6* for LEGEND.

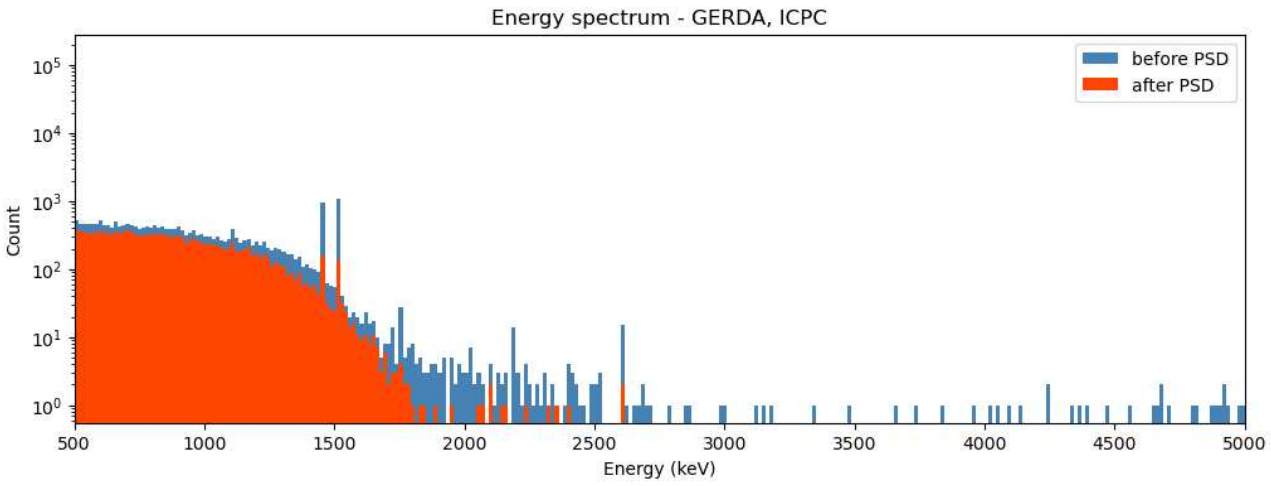

Figure 4.1: *Energy spectrum of ICPC detectors in GERDA*

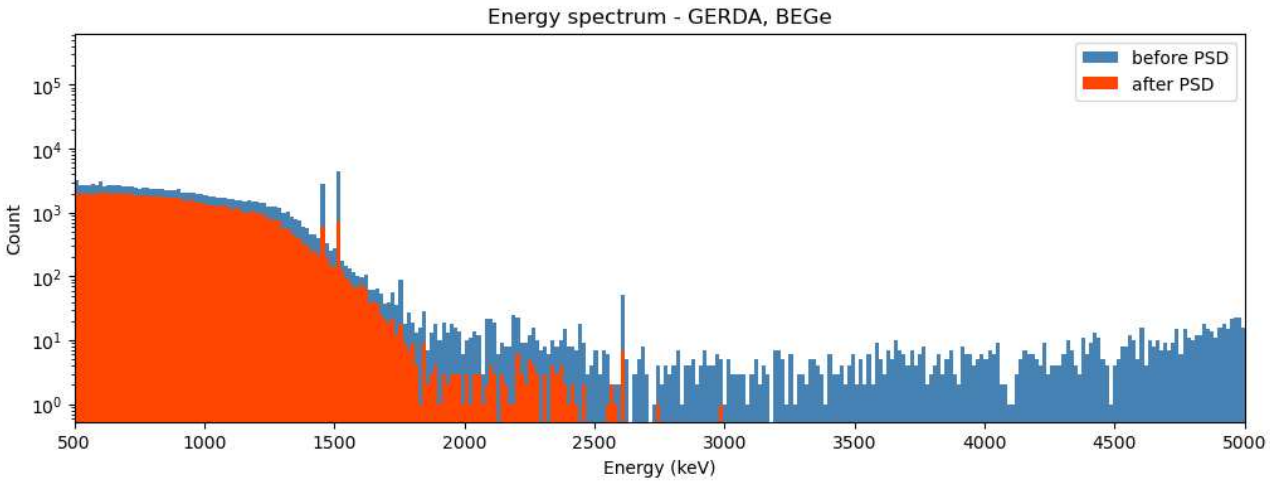

Figure 4.2: *Energy spectrum of BEGe detectors in GERDA*

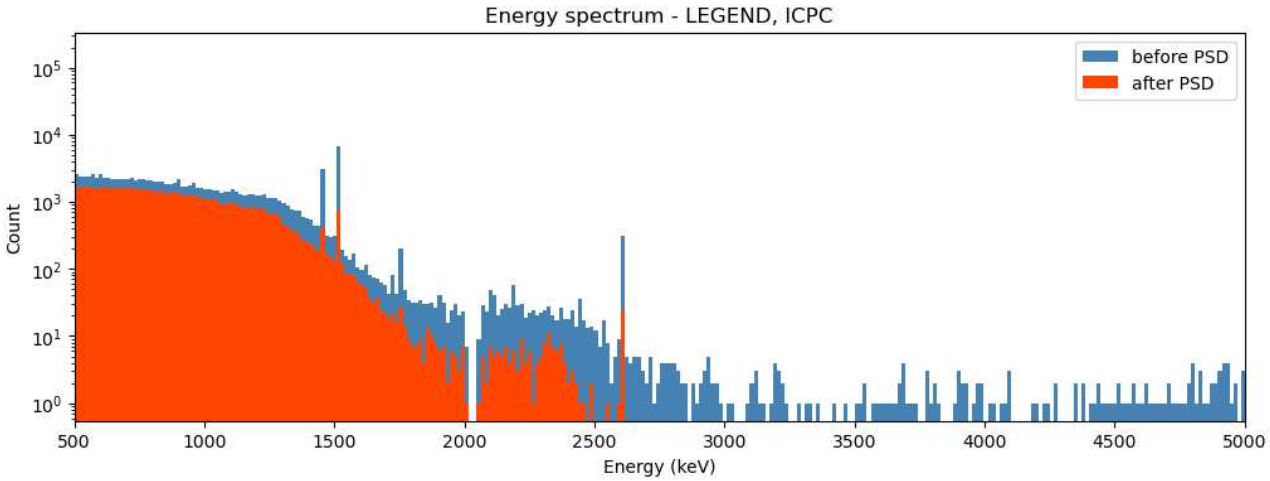

Figure 4.3: *Energy spectrum of ICPC detectors in LEGEND*

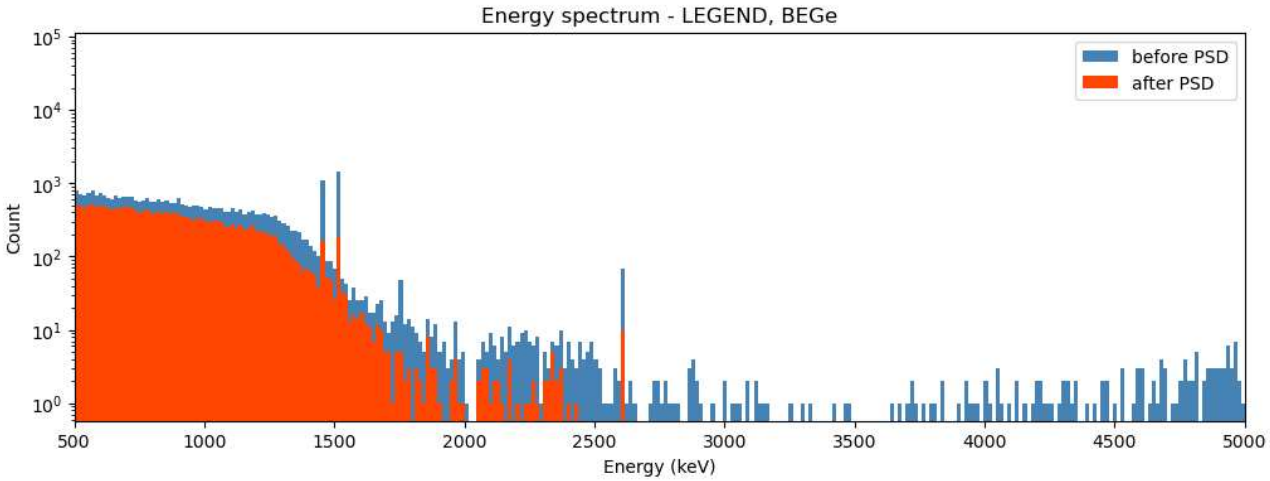

Figure 4.4: *Energy spectrum of BEGe detectors in LEGEND*

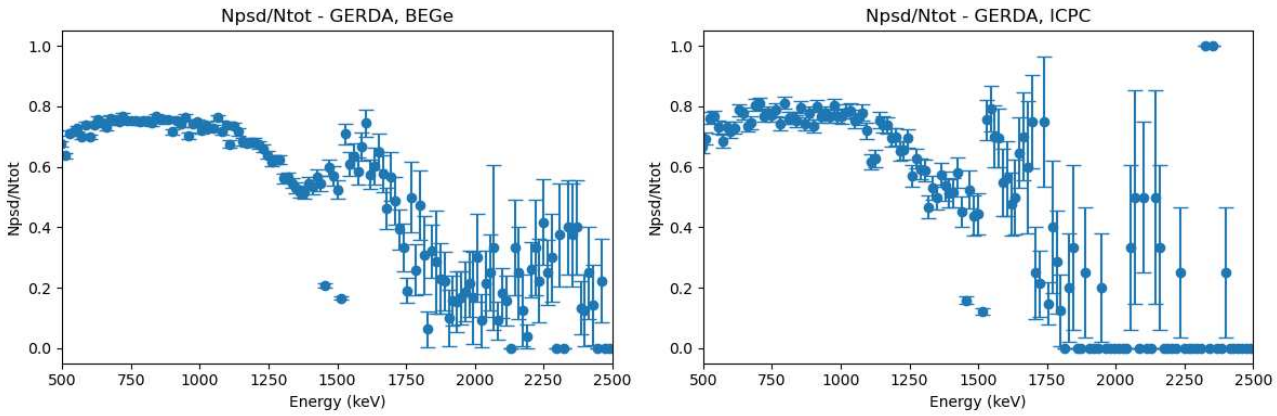

Figure 4.5: *Bin-by-bin ratios of the post-PSD spectrum to the pre-PSD spectrum in GERDA*

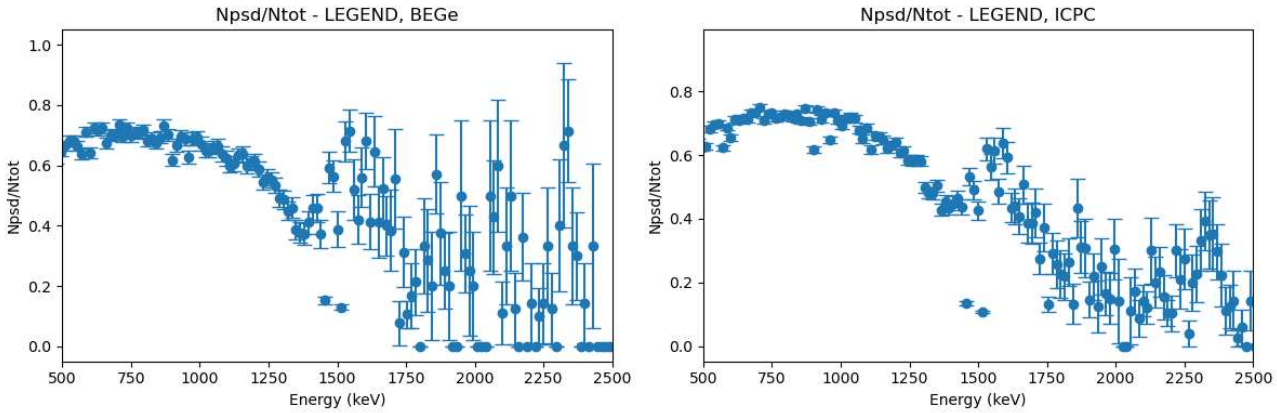

Figure 4.6: *Bin-by-bin ratios of the post-PSD spectrum to the pre-PSD spectrum in LEGEND*

In the graphs of *Figure 4.5* and *Figure 4.6*, the difference between the ratios $\frac{N_{post-PSD}}{N_{pre-PSD}}$ in the range 0keV-1500keV and those in the range 1500keV-2500keV is evident: the former are well localized and have acceptable error bars, while the latter exhibit large random oscillations and are associated with very large errors. This is due to the reduced sample size beyond a certain energy level. For this reason, these two regions of the spectrum are studied separately and in different ways.

It should also be noted that, for the following considerations, it is necessary to delve into the various contributions that make up the energy spectra. For this purpose, *Figures 4.7 and 4.8* are presented. These represent the background models of the GERDA spectra (BEGe detectors) and LEGEND-200 (all detectors) obtained through Monte Carlo simulations. Firstly, it is observed that alpha particles represent almost all events above 3000keV, both in GERDA and LEGEND-200. By comparing with the spectra in *Figures 4.1, 4.2, 4.3, and 4.4*, it can be concluded that the PSD cut operates particularly effectively on this type of event in this part of the spectrum, as most of them do not survive this filter.

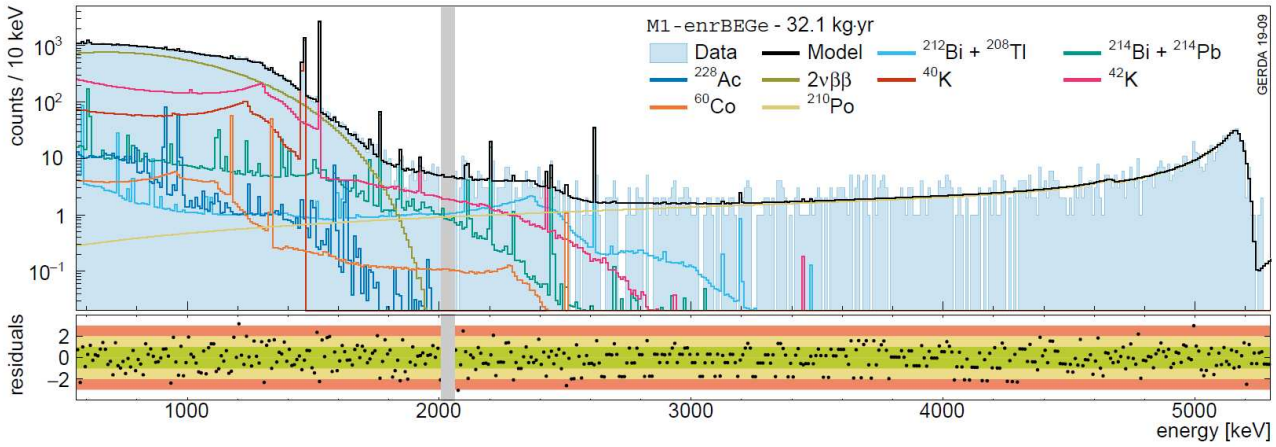

Figure 4.7: *Background model of the spectrum of BEGe detetors in GERDA. The gray band corresponds to a +-25 keV wide band around the Qbb excluded from the analysis (blinded region). Picture from [5]*

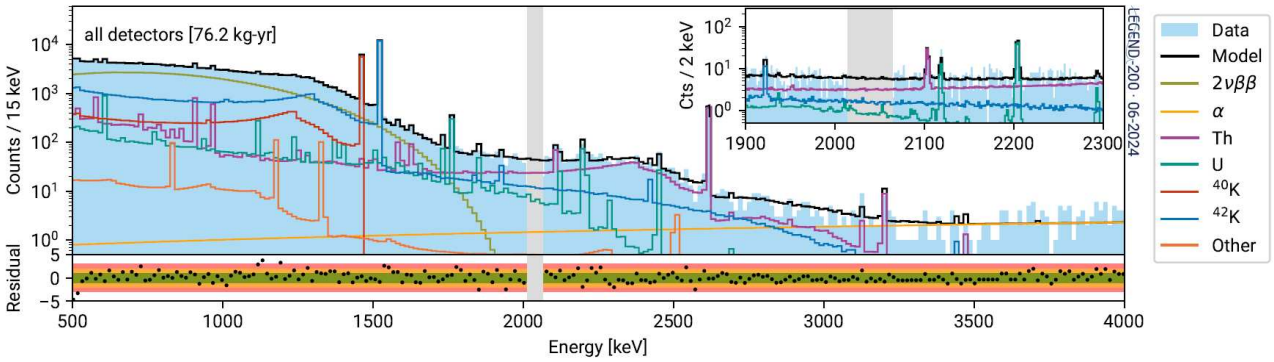

Figure 4.8: *Background model of the spectrum of LEGEND-200. The gray band corresponds to a +-25 keV wide band around the Qbb excluded from the analysis (blinded region).*

Due to the different background composition along the energy spectrum, we decided to split the analysis in two energy regions: from 700 keV to 1300 keV and from 1930 keV to 2190 keV. The first region (see *Figure 4.7* and *Figure 4.8*) is dominated by $2\nu\beta\beta$ events. These events are Single Site Events similar to the signal. The PSD should not touch these events (SF 90%), while it should eliminate the remaining background events. *Figure 4.9* shows the results for BEGe and ICPC separetely.

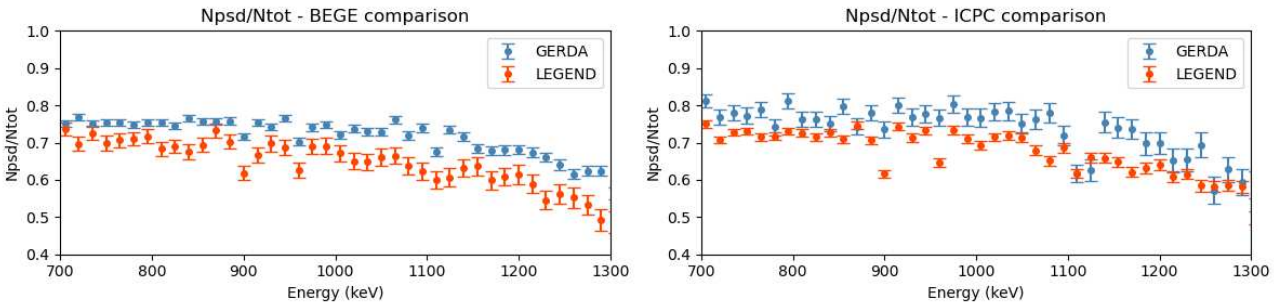

Figure 4.9: *Comparison of the bin-by-bin ratios of the spectra of GERDA and LEGEND-200 in [700,1300] keV*

From these plots it seems that PSD perfoms better in LEGEND-200 than in GERDA in this region of the spectrum.

The second energy region taken under consideration is the region around the $Q_{\beta\beta}$. From the *Figure 4.7* and *Figure 4.8*, giving a look to the gray bands (the blinded region: $Q_{\beta\beta} \pm 25keV$), one can realize clearly that the backgorund composition is different in GERDA respect to LEGEND-200. Specifically, it is noted that in the blinded region, GERDA has a significant contribution from ^{210}Po α particles, and then contributions from ^{214}Bi, ^{212}Bi, ^{208}Tl, ^{214}Pb, ^{42}K, and, to a lesser extent, ^{60}Co. For the LEGEND-200 detectors, however, α particles play a secondary role, while the major contributors are Thorium, Uranium, and ^{42}K. For each of these contributions, the PSD has different rejection capabilities, complicating a comparison between LEGEND-200 and GERDA based on the Survival Fraction calculation. For this reason, it was decided to use the Background Index (BI) as an indicative value of the effectiveness of the PSD cuts. This is defined as:

$$BI = \frac{N^{post-cuts}_{background}}{\mathcal{E} \cdot \Delta E}$$

where $N^{post-cuts}_{background}$ is the number of background events remaining after the application of the selection cuts (it should be noted that only the PSD cut was applied, not the Liquid Argon Veto cut), $\mathcal{E}$ is the exposure - a parameter given by the product of the detector mass and the data acquisition time - and ΔE is the considered energy range. A low BI is essential to increase the sensitivity of the experiment to the detection of rare events such as $0\nu\beta\beta$. The lower the BI, the lower the probability that background events will cover the expected signal region.

In this case, ΔE is given by the standard interval [6] used to study the region around $Q_{\beta\beta}$, namely the range 1930keV-2190keV excluding the blinded zone and the intervals (2104±5)keV and (2119±5)keV that contain two known background gamma peaks. The Background Index was then calculated as shown in *Table 4.1*:

	GERDA		LEGEND-200	
	BEGe	ICPC	BEGe	ICPC
$N^{post-cuts}_{background}$	31	5	25	67
ΔE [keV]	190	190	190	190
$\mathcal{E}$ [kg·yr]	53.4	8.5	11.0	45.9
BI [kev^{-1}·kg^{-1}·yr^{-1}]	$(3.1 \pm 0.5) \cdot 10^{-3}$	$(3.1 \pm 1.4) \cdot 10^{-3}$	$(12.0 \pm 2.4) \cdot 10^{-3}$	$(7.7 \pm 0.9) \cdot 10^{-3}$

Table 4.1: *Background Index calculation after PSD-cuts only*

Based on these results one might conclude that the PSD works better in GERDA than in LEGEND-200. But as we observed the background composition is different and the survival fractions of the PSD depend by the type of events (gammas from Th and U differ from electrons coming from ^{42}K). Moreover, if one gives a look to the BI before PSD cuts (*Table 4.2*) one can see that, unfortunately,

LEGEND-200 has a higher contamination (problem which is under active investigation from the collaboration). Additionally, GERDA data come from a completed experimental project, so it can be assumed that it represents the optimal conditions achievable with that instrumentation. LEGEND-200, on the other hand, is still in development, so these results are expected to improve in the years to come.

	GERDA		LEGEND-200	
	BEGe	ICPC	BEGe	ICPC
$N_{background}^{pre-cuts}$	170	32	86	370
ΔE [keV]	190	190	190	190
$\mathcal{E}$ [kg·yr]	53.4	8.5	11.0	45.9
BI [kev^{-1}·kg^{-1}·yr^{-1}]	$(1.7 \pm 0.1) \cdot 10^{-2}$	$(2.0 \pm 0.4) \cdot 10^{-2}$	$(4.1 \pm 0.4) \cdot 10^{-2}$	$(4.2 \pm 0.2) \cdot 10^{-2}$

Table 4.2: *Background Index calculation berfore PSD-cuts*

5 Conclusion

The work presented in this paper aims to investigate Pulse Shape Discrimination in LEGEND-200. This study was conducted by first analyzing the calibration data spectrum to assess the stability of PSD over time and among detectors. Subsequently, a comparison was made using physics data from GERDA and LEGEND-200.

From the analysis of the calibration data, the ability of PSD to discriminate between Multi-Site Events (MSEs) and Single-Site Events (SSEs) based on the charge pulse shape generated by events is evident. Furthermore, the following observations were made:

- The efficiency of PSD is directly related to the volume (and hence the mass) of the detectors: larger detectors are more capable of identifying MSEs.
- Issues related to the instability of Survival Fractions caused by GERDA's electronics layout have been resolved in LEGEND-200.
- Based on data collected by LEGEND-200 over the past year, Pulse Shape Discrimination appears to be a stable technique over time.

From the analysis of the physics data, excellent performance of PSD in eliminating α particle events has been observed, along with an improvement in background reduction in the 700keV-1300keV region of $2\nu\beta\beta$ decays compared to GERDA. Regarding the region of interest around $Q_{\beta\beta}$, it was noted that PSD analysis cannot disregard observations on the nature of event contributions that build the spectrum. Additionally, by calculating the Background Index relative to the PSD-cut in the region of interest, the sensitivity level achieved by PSD in LEGEND-200 has been quantified and compared to GERDA's sensitivity level at the end of its operation.

Bibliography

[1] Super-Kamiokande collaboration. Evidence for Oscillation of Atmospheric Neutrinos. In: *Phys. Rev. Lett. 81, 8* (1998). URL: https://doi.org/10.1103/PhysRevLett.81.1562.

[2] LEGEND collaboration. The Large Enriched Germanium Experiment for Neutrinoless $\beta\beta$ Decay: LEGEND-200 at LNGS. In: *The LEGEND-200 LNGS proposal - P 58/18* (2018).

[3] Comellato T., Agostini M., and S. Schönert. Charge-carrier collective motion in germanium detectors for $\beta\beta$-decay searches. In: *Eur. Phys. J. C 81, 76* (2021). URL: https://doi.org/10.1140/epjc/s10052-021-08889-0.

[4] GERDA collaboration. Pulse shape analysis in GERDA Phase II. In: *Eur. Phys. J. C 82, 284* (2022). URL: https://doi.org/10.1140/epjc/s10052-022-10163-w.

[5] GERDA collaboration. Modeling of GERDA Phase II data. In: *J. High Energ. Phys. 2020, 139* (2020). URL: https://doi.org/10.1007/JHEP03(2020)139.

[6] GERDA collaboration. Final Results of GERDA on the Search for Neutrinoless Double-β Decay. In: *Phys. Rev. Lett. 125, 252502* (2020). URL: https://doi.org/10.1103/PhysRevLett.125.252502.

[7] Michelle J. Dolinski, Alan W. P. Poon, and Werner Rodejohann. Neutrinoless Double-Beta Decay: Status and Prospects. In: *Annual Reviews* (2019). URL: https://doi.org/10.48550/arXiv.1902.04097.

[8] GERDA collaboration. The GERDA experiment for the search of $0\nu\beta\beta$ decay in ^{76}Ge. In: *Eur. Phys. J. C 73, 2330* (2013). URL: https://doi.org/10.1140/epjc/s10052-013-2330-0.

[9] GERDA collaboration. Upgrade for Phase II of the GERDA experiment. In: *Eur. Phys. J. C 78, 388* (2018). URL: https://doi.org/10.1140/epjc/s10052-018-5812-2.

[10] LEGEND collaboration. LEGEND-1000 Preconceptual Design Report. 2021. URL: https://doi.org/10.48550/arXiv.2107.11462.

[11] Saleh G. First analysis of LEGEND-200 commissioning data: searching for neutrinoless double beta decay in Germanium-76. 2023. URL: https://thesis.unipd.it/handle/20.500.12608/48928.

[12] GEDA collaboration. Liquid argon light collection and veto modeling in GERDA Phase II. In: *Eur. Phys. J. C 83, 319* (2022). URL: https://doi.org/10.1140/epjc/s10052-023-11354-9.